Derivative expansion for computing critical exponents of O(N) symmetric models at next-to-next-to-leading order

Zoltán Péli *
MTA-DE Particle Physics Research Group, H-4010 Debrecen, P.O. Box 105, Hungary

(Received 14 October 2020; revised 22 January 2021; accepted 4 March 2021; published 22 March 2021)

We apply the derivative expansion of the effective action in the exact renormalization group equation up to fourth order to the Z_2 and O(N) symmetric scalar models in $d = 3$ Euclidean dimensions. We compute the critical exponents ν, η, and ω using polynomial expansion in the field. We obtain our predictions for the exponents employing two regulators widely used in exact renormalization group computations. We apply Wynn's epsilon algorithm to improve the predictions for the critical exponents, extrapolating beyond the next-to-next-to-leading order prediction of the derivative expansion.

DOI: 10.1103/PhysRevE.103.032135

I. INTRODUCTION

In this work we compute the critical exponents ν, η, and ω for the Z_2 and O(N) symmetric scalar models in $d = 3$ Euclidean dimensions. We use the exact renormalization group (ERG) equation for effective average action [1]. The ERG is a highly versatile method for tackling problems in statistical physics and quantum field theory. Its modern formulation has sprouted from Wilson's approach to renormalization [2].

There are a number of other ways in modern physics to obtain critical exponents. Perhaps the first one to come to mind is lattice simulation. The Monte Carlo (MC) simulations provide one of the most precise determinations of the exponents for the Ising [3] and XY [4] universality classes. Generally, a larger lattice yields more precise predictions, but also increases the computational effort. The most commonly applied method in quantum field theory is the loop expansion, which requires a smallness of the couplings in the Lagrangian. In fixed $d = 3$ dimensions, the Ising exponents have been computed up to six-loop order [5] and the β functions are determined at seven loops [6]. Wilson's $d = 4 - \epsilon$ expansion has also been applied up to ϵ^6 [7]. Presently, the most precise computation for the Ising exponents comes from the conformal bootstrap method (CB) [8] using conformal field theory. This method also has a high computational cost (see Table II. of [9], for instance). The last highlight on this list is the large-N expansion. It is applicable on theories, where the symmetry group corresponding to the symmetry of the Lagrangian is O(N), SO(N), SU(N), and so on.

The ERG is formulated in terms of functional equations, which are in general very hard to solve. In order to tackle this difficulty, a precise approximation scheme has to be applied, which is most often the so-called derivative expansion (DE). The DE consists of expanding the action in terms of the gradient of the field. This approximation scheme contains no explicit small parameter, thus its convergence has been questioned. Recently, however, arguments have been put forward that the DE is indeed convergent [10] at least for the Z_2 and O(N) symmetric models. The corrections were shown to be dampened by a factor of $1/4-1/9$, depending on the regulator function. The physical predictions depend on the regulator function at fixed order in the DE. This is similar to the renormalization scale dependence in perturbative quantum field theory.

Here we compute the critical exponents at the next-to-next-to-leading order (NNLO) of the DE on the Z_2 symmetric scalar model as a benchmark and then generalize the computations to the O(N) symmetric models. Our results complement those of Ref. [11], where the authors employ the DE at NNLO as well, but there are key differences: (i) we do not use truncation of momenta in the derivation of our β functions and (ii) we employ Taylor expansion of the β functions in the field. These β functions describe the scale dependence of different functions depending on the field. The Taylor expansion reduces these to the β functions for coupling strengths corresponding to different vertices of the field. We compute the exponents with the exponential regulator, which is applicable at any order of the derivative expansion and (iii) also with a Θ-type regulator [12], which is the simplest applicable regulator at NNLO. The critical exponents of the Z_2 symmetric model have already been computed in Ref. [13] using Taylor expansion in the field, although with a more severe truncation of the Taylor series.

By increasing the number of terms in the Taylor expansion of the scale-dependent functions, the values of the critical exponents fluctuate and eventually stabilize around their limiting values. Reassuringly, similar behavior has been observed in Ref. [13]. Interestingly, we find that the exponents ν, η, and ω of the O(N) symmetric model are estimated remarkably well even at the zeroth order of the Taylor expansion in the field variable of the scale-dependent functions corresponding to the NNLO of the DE. Furthermore, this fluctuation of the exponents at the NNLO is much less pronounced in the O(N) symmetric case than in the the Z_2 symmetric one. This dampening of the fluctuation is likely the result of

*zoltanpeli92@gmail.com

having more scale-dependent functions for the O(N) symmetric models than for the Z_2 symmetric one. These scale-dependent functions have to interplay in such a way that the predictions for the exponents are in good agreement with other method's predictions. This is true for at least large values of N, where the higher order contributions from the DE are expected to be very small as the leading order of the DE becomes exact in the limit $N \to \infty$ [14].

We introduce the ERG briefly in Sec. II. The procedure we use to acquire the results is outlined in Sec. III. Our findings for the Z_2 symmetric model are detailed in Sec. V, while those of the O(N) symmetric one can be found in Sec. VI.

II. EXACT RENORMALIZATION GROUP

The ERG uses functional integrodifferential equations to describe the dependence of a theory on the variation of the characteristic energy scale. These equations can be used to describe nonperturbative phenomena. A widely used form of the ERG is the Wetterich equation [1], which describes the scale dependence of the effective average action:

$$\dot{\Gamma}_k = \tfrac{1}{2}\mathrm{STr}\big[\dot{R}_k\big(\Gamma_k^{(2)} + R_k\big)^{-1}\big], \tag{1}$$

where the dot is an abbreviation for the operation $k\partial_k$. The functional Γ_k is the Legendre transform of the generating functional of the connected Green's functions plus a scale-dependent mass term, called the regulator function R_k, and $\Gamma_k^{(2)}$ is the inverse propagator containing the physical mass. All the different formulations of the ERG equations require some sort of regularization. The regulator vanishes in the low-energy limit of the theory. The supertrace contracts all momenta and group indices, therefore this equation can be viewed as a one-loop expression with an operator insertion ($\dot{R}_k$) and no external legs. The functional Γ_k possesses the linear symmetries of the original Lagrangian if the regulator also does. In order to solve Eq. (1), one has to make an ansatz for Γ_k comprised of a finite number of functions, consistent with the symmetries of the original theory, and specify the regulator function.

A widely used approach in terms of the ansatz is the derivative expansion. In this method, the leading order (or local potential approximation, LPA) only has a scale-dependent potential and a canonical kinetic term. An important feature of the exact renormalization group is that even the irrelevant couplings acquire nontrivial scale dependence during the renormalization group (RG) flow. This observation leads one to believe that the LPA prediction can be improved by including couplings, corresponding to scale-dependent functions, which multiply all operators but the unit operator. Consequently, the next-to-leading order (NLO) introduces scale-dependent functions multiplying every independent operator with two derivatives. Similarly, at the NNLO operators with four derivatives appear. This expansion makes the functional space of Γ_k less and less truncated order by order and at the same time increases the number of terms in the truncated ansatz. One expects that including higher orders in the derivative expansion improves the quality of the physical predictions. In fact, the convergence of this method has been demonstrated in Ref. [10] up to N^{3}LO for the Z_2 universality class.

The dependence on the regulator is expected to vanish in the low-energy limit, $k \to 0$. As we study the critical theory, which is scale independent, we expect our physical predictions to be independent of the specific form of the regulator R_k. This is strictly true only if we do not truncate the functional space. The dependence of the physical predictions and the magnitude of this spurious dependence on the regulator is somewhat similar to the renormalization scale dependence in the perturbative quantum field theory.

III. DERIVING THE β FUNCTIONS

The system is critical in the Wilson-Fisher fixed point, which is the nontrivial solution of the fixed-point equation of the β functions. We need to obtain the β functions and the Wilson-Fisher fixed point to compute the critical exponents. The derivation of these β functions is comprised of four steps for a given ansatz: (i) splitting the field to homogeneous and fluctuating pieces, (ii) functional Taylor expansion of Eq. (1) in powers of the fluctuating field, (iii) expansion in the momenta corresponding to the fluctuating field, and finally (iv) classification and sorting of the different types of loop integrals, called threshold integrals. We automated these steps in a *Mathematica* code attached in the Supplemental Material [15].

A. Functional and momentum expansions

As an example, let us consider the ansatz for the Z_2 symmetric scalar model at the NLO of the DE:

$$\Gamma_k[\phi] = \frac{1}{2}\int_x Z_k(\rho_x)(\partial\phi_x)^2 + \int_x U_k(\rho_x), \tag{2}$$

where $\rho_x = \phi_x^2/2 \equiv \phi(x)^2/2$, $\int_x \equiv \int d^dx$ (and similarly $\int_p = (2\pi)^{-d}\int d^dp$, to be used later), and $(\partial f)^2 \equiv (\partial_\mu f)(\partial^\mu f)$ for any f. The flow for U_k is obtained by setting the field ϕ to be homogeneous $\phi_x = \Phi$ (meaning $\partial\Phi = 0$) and solving Eq (1). In order to find $\dot{Z}_k(\rho \equiv \Phi^2/2)$ however, we expand Eq. (1) in terms a fluctuating field η_x around a constant background $\phi_x = \Phi + \eta_x$ and collect the terms proportional to $\mathcal{O}(\eta^2)$. In momentum space, this is given by

$$\begin{aligned}\int_Q &(\dot{Z}_k(\rho)Q^2 + \dot{U}_k'(\rho) + 2\rho\dot{U}_k''(\rho))\eta_Q\eta_{-Q}\\ &= \int_{p,r}\dot{R}_k(p^2)\mathcal{G}(p^2)\big(\eta\Gamma^{(3)}\big)_{p,-r}\mathcal{G}(r^2)\big(\eta\Gamma^{(3)}\big)_{r,-p}\mathcal{G}(p^2)\\ &\quad - \frac{1}{2}\int_p \dot{R}_k(p^2)\mathcal{G}(p^2)\big(\eta\Gamma^{(4)}\eta\big)_{p,-p}\mathcal{G}(p^2),\end{aligned} \tag{3}$$

with $\mathcal{G}(p^2)$ being the regularized propagator $[(\Gamma_k^{(2)} + R_k)^{-1}]$, $r = p \pm Q$, and

$$\begin{aligned}\big(\eta\Gamma^{(3)}\big)_{p,q} &= \eta_{-p-q}\frac{\delta^{(3)}\Gamma}{\delta\phi_p\delta\phi_q\delta\phi_{-p-q}}\bigg|_{\phi_x=\Phi},\\ \big(\eta\Gamma^{(4)}\eta\big)_{p,q} &= \int_Q \eta_Q\frac{\delta^{(4)}\Gamma}{\delta\phi_p\delta\phi_q\delta\phi_Q\delta\phi_{-Q}}\bigg|_{\phi_x=\Phi}\eta_{-Q}.\end{aligned} \tag{4}$$

Generally, in order to find $\dot{F}$, where F multiplies an operator with n derivatives one has to collect terms proportional to

$\mathcal{O}(\eta^n)$. We denote the momentum of the fluctuating field η with Q for transparency. In case there are multiple η fields in the same expression, their momenta are denoted with Q_1, Q_2, and so on.

The left-hand side of Eq. (3) shows, that in order to obtain $\dot{Z}_k(\rho)$, we have to expand the right-hand side in Q_μ up to Q^2 and finally, identify the terms proportional to Q^2 as the β function of $Z_k(\rho)$. The computations become naturally more complicated at NNLO, since then there are multiple momenta Q_i. For the sake of concreteness, the complete ansatz for the Z_2 symmetric scalar model at the fourth order of the derivative expansion reads as

$$\begin{aligned}\Gamma_k[\phi] = &\frac{1}{2}\int_x Z_k(\rho_x)(\partial\phi_x)^2 + \int_x U_k(\rho)\\ &+ \frac{1}{2}\int_x W_k(\rho_x)(\partial_\mu\partial_\nu\phi_x)^2\\ &+ \frac{1}{2}\int_x H_k(\rho_x)\phi_x(\partial\phi_x)^2(\partial^2\phi_x) + \frac{1}{2}\int_x J_k(\rho_x)(\partial\phi_x)^4.\end{aligned} \tag{5}$$

This form has been studied in great detail without and also with expansion in the fields [10,13]. The scale-dependent functions W_k, H_k, and J_k are obtained from Γ_k via

$$W_k(\rho) = \lim_{Q_1\to 0}\left(\frac{\partial}{\partial Q_1^2}\right)^2 \Gamma^{(2)}_{Q_1,Q_2}, \tag{6}$$

$$H_k(\rho) = -\frac{1}{2\Phi}\lim_{Q_1,Q_2\to 0}\frac{\partial}{\partial Q_1^2}\frac{\partial}{\partial Q_2^2}\Gamma^{(3)}_{Q_1,Q_2,Q_3}, \tag{7}$$

$$J_k(\rho) = -\frac{1}{4}\lim_{Q_1,Q_2,Q_3\to 0}\frac{\partial}{\partial Q_1^2}\frac{\partial}{\partial (Q_2Q_3)}\Gamma^{(4)}_{Q_1,Q_2,Q_3,Q_4}, \tag{8}$$

as the coefficients of the integrands in the integrals $\int_{Q_1,\ldots,Q_n}\prod_{i=1}^n \eta_{Q_i}\delta(\sum_{i=1}^n Q_i)$ for $n = 2$, 3, and 4. Note, that the scale-dependent functions can be acquired by any permutation of the momentum indices Q_i in the differentiation.

The O(N) symmetric models introduce an additional index on the field corresponding to the symmetry group and can be generalized from the Z_2 symmetric models in a straightforward way. The complete ansatz used in this work is given in Eq. (23). A slightly different, but equivalent ansatz is used in Ref. [11].

B. Threshold integrals

After sorting the different types of $\int_p$ integrals that appear in the formula of a general $\dot{F}_k$ in the Z_2 symmetric model at NNLO, one finds three such types:

$$L_m^{d+a} = \int_p p^a \frac{\dot{R}_k(p^2)}{G(p^2)^m}, \tag{9}$$

$$M_{m,b}^{d+a,\beta} = \int_p p^a\left[\partial_{p^2}^\beta G(p^2)\right]^b \frac{\dot{R}_k(p^2)}{G(p^2)^m}, \tag{10}$$

$$N_{m,b,c}^{d+a,\beta,\gamma} = \int_p p^a\left[\partial_{p^2}^\beta G(p^2)\right]^b\left[\partial_{p^2}^\gamma G(p^2)\right]^c \frac{\dot{R}_k(p^2)}{G(p^2)^m}, \tag{11}$$

where m, b, c, β, and γ are positive integers and a is a non-negative one. We have also introduced $G(p^2)$ as the regularized inverse propagator $[(\Gamma_k^{(2)} + R_k)]$. As we consider the NNLO of the DE, derivatives of the inverse propagator appear up to the fourth derivative. This yields the constraint $b\beta + c\gamma \leqslant 4$ for the threshold integral parameters.

In the O(N) symmetric models two types of propagators appear: one massive and one corresponding to the $N-1$ Goldstone modes. This proliferates the types of threshold integrals.

C. Regulator functions

The regulator itself is a function of the loop momentum squared p^2 and the running scale k. It is usually expressed as the function of the dimensionless ratio $y = p^2/k^2$:

$$R_k(p^2) = Z_k k^2 y\, r(y), \tag{12}$$

where the explicit form of the regulator is defined by the function $r(y)$, $Z_k = 1$ at LPA and $Z_k \equiv Z_k(\rho = \rho^*)$ at higher orders of the DE with ρ^* being a reference value, detailed in Sec. III D. In general, the form of the regulator is very flexible, yet it has to obey some requirements [1].

In order to obtain numerical results, one has to specify the regulator function. In this work we use two different types. The Θ_2 regulator introduced in Ref. [12] reads as

$$r_\Theta(y) = \alpha\frac{(1-y)^2}{y}\Theta(1-y), \tag{13}$$

where $\Theta(x)$ is the Heaviside step function. The regulator (13) is the simplest possible regulator which can be used in ∂^4-order calculations. The caveat is that it is not applicable beyond ∂^4 order due to the appearance of undefined Dirac-delta functionals $[\delta(0)]$ in the final equations. Generally, at ∂^n order the integral containing the highest G derivative is

$$M_{m,1}^{d,n} = \frac{\Omega_d}{(2\pi)^d}k^d\int dy\, y^{-1+d/2}\left[\partial_y^n G(y)\right]\frac{\dot{R}_k(y)}{G(y)^m}, \tag{14}$$

where we have changed to the variable $y = p^2/k^2$. For the regulator (13) and $n = 4$ this integral takes the form

$$\begin{aligned}M_{m,1}^{d,4} &= -4\alpha^2\frac{\Omega_d}{(2\pi)^d}\left(Z_k^2 k^{d+2}\right)\\ &\quad\times\int dy\frac{y^{-1+d/2}(y^2-1)\Theta(1-y)}{G(y)^m}\delta'(1-y)\\ &\equiv 4\alpha^2\left(Z_k^2 k^{d+2}\right)\frac{\Omega_d}{(2\pi)^d}\frac{1}{G(1)^m}.\end{aligned} \tag{15}$$

This integral is ambiguous in the sense that the result is obtained by integration by parts and then defining $\Theta(0)$ to be 1/2. This ambiguity is lifted when one considers (13) as the limit of a C^∞-type regulator function, such as (A1). The process to do so is detailed in Appendix A. The integrals, which contain $\partial_y^3 G_k(y) = -2\alpha(Z_k k^2)\delta(1-y)$ vanish, because the distributional product $x\delta(x)$ is zero and every integral contains $(1-y)$ through $\dot{R}_k(y)$.

The second regulator we use here is called the exponential regulator

$$r_{\exp}(y) = \alpha\frac{e^{-y}}{y}, \tag{16}$$

which is a C^∞ function and has the advantage over the regulator containing the Θ function that it can be used at any

orders of the derivative expansion. Both r_Θ and $r_{\rm exp}$ remain unchanged in the Z_2 and O(N) symmetric scalar models.

We vary the value of α and compute its effect on the critical exponents. We consider the extrema of these functions as the optimal values in our final predictions. This is the implementation of the principle of minimal sensitivity (PMS) [16,17]. In practice, we locate the Wilson-Fisher fixed point for a fixed regulator for several values of α, which simultaneously yields $\eta(\alpha)$ as the anomalous dimension is just a function of the couplings in the model. In each case we applied the PMS, $\eta(\alpha)$ is either an upside or downside facing paraboloid. The optimal value of $\eta^{\rm opt}$ is the minimum or maximum of this paraboloid at $\alpha^{\rm opt}$ and we accept $\nu(\alpha^{\rm opt})$ and $\omega(\alpha^{\rm opt})$ as $\nu^{\rm opt}$ and $\omega^{\rm opt}$. In this sense, we only apply the PMS on the anomalous dimension.

D. Polynomial expansion and exponents

In order to compute the critical exponents one has to use dimensionless quantities. The mass dimension of some are given as

$$[\phi] = (d - 2 + \eta_k)/2, \quad [U] = d, \tag{17}$$

where η_k is the running anomalous dimension, which is defined by

$$\eta_k = -k\,\partial_k \ln Z_k(\rho^*). \tag{18}$$

The running anomalous dimension becomes the critical exponent η in the fixed point. The Euclidean dimension d is a continuous parameter in the β functions of the dimensionless couplings. We set its value to $d = 3$ throughout this work. The β functions for the dimensionless scale-dependent functions are partial differential equations with the scale k and the dimensionless field $\tilde{\rho}$ (we denote the dimensionless quantities with a tilde) as independent variables. One strategy to solve these equations is to Taylor expand the dimensionless scale-dependent functions in power of the dimensionless field around a reference point ρ^*

$$\tilde{F}_k(\tilde{\rho}) = \sum_{n=0}^{M_F} \frac{\tilde{f}_n(k)}{n!}(\tilde{\rho} - \rho^*)^n. \tag{19}$$

This reduces the coupled set of partial differential equations to a coupled set of ordinary differential equations. This course of action has been taken, for example, in Refs. [13,17]. There are two well-known choices for ρ^*. It can either be zero ($\rho^* = 0$) or the running minimum $\rho^* = \kappa_k$ of the most basic scale-dependent function, the local potential U_k. Throughout this work we use $\rho^* = \kappa_k$, because it provides a faster convergence of the physical results with increasing M_F than expanding around the vanishing field [18,19]. We denote the highest power in the Taylor series of a general scale-dependent function F_k with M_F; if the subscript contains multiple capital Latin letters such as M_{WHJ}, it means that the scale-dependent functions W_k, H_k, and J_k are truncated at identical powers $M_W = M_H = M_J \equiv M_{WHJ}$.

The Wilson-Fisher fixed point is the nontrivial fixed-point solution of the β functions. Once it is located, the critical value of the anomalous dimension η is determined. The critical exponent of the correlation length ν and its subleading scaling corrections ω, ω_i are obtained by linearizing the RG flow in the vicinity of the fixed point. The eigenvalues of the Jacobian matrix $J_{ij} = \partial\beta_{\tilde{g}_i}/\partial\tilde{g}_j$, with $\tilde{g}_i$ being a general dimensionless coupling from the model, at the fixed point are $-\nu^{-1} < \omega < \omega_1 < \ldots$ in increasing order.

The polynomial expansion gives very good predictions at $d = 3$ as demonstrated in Ref. [13]. However, this might not be the case for $d < 3$. As d is lowered, new couplings g_n corresponding to the vertex ϕ^{2n} become marginal ($[g_n] = 0$) at $n = d/(d-2)$. If g_{n+1} is marginal, then g_n is relevant. At $d = 4$ only the mass squared is a relevant coupling ($[g_1] > 0$) and the quartic interaction is marginal ($[g_2] = 0$). At $d = 3$ there are two relevant couplings ($[g_1] > 0$ and $[g_2] > 0$) and thus a nontrivial fixed point, the Wilson-Fisher fixed point, appears. At $d = 8/3$ the coupling g_3 also becomes relevant and introduces a new nontrivial fixed point besides the Wilson-Fisher one. This makes finding the Wilson-Fisher fixed point much more difficult. In particular, in Ref. [20] it has been found that the Euclidean action is not bounded from below in the fixed point, which sets a bound on the applicability of the polynomial expansion.

IV. WYNN'S EPSILON ALGORITHM

In many instances, the prediction of an exponent X at successive orders of the DE, $X_{\rm LPA}$, $X_{\rm NLO}$, $X_{\rm NNLO}$, and so on, form a convergent series alternating around the exact value X. This has been discussed in great detail in Ref. [10]. In Ref. [11] the authors use the small parameter $1/4 - 1/9$ of the DE to improve their predictions on the critical exponents of the O(N) symmetric scalar models at NNLO of the DE.

One may also turn to a similar, yet different approach to improve exponent predictions in the derivative expansion. Several series acceleration methods exist and are used successfully to accurately compute the limit of a slowly converging sequence. One of the most robust of these algorithms is Wynn's epsilon algorithm [21,22]. It is already applicable if one only has the first three elements a_1, a_2, a_3 of a sequence (a_n). In that case, the third element is improved as

$$\tilde{a}_3 = a_2 + \frac{1}{-\frac{1}{-a_1+a_2} + \frac{1}{-a_2+a_3}} = \frac{-a_2^2 + a_1 a_3}{a_1 - 2a_2 + a_3}. \tag{20}$$

Given the critical exponent X, this means, that the improved prediction of the DE is

$$\tilde{X} = \frac{-X_{\rm NLO}^2 + X_{\rm LPA} X_{\rm NNLO}}{X_{\rm LPA} - 2X_{\rm NLO} + X_{\rm NNLO}}. \tag{21}$$

The formula is even simpler for the anomalous dimension as the LPA prediction for it is zero. We employ Wynn's algorithm when it works the best, i.e., with alternating sequences. The ERG predictions for the O(N) critical exponents at different orders of the DE show that while the predictions for ν and η do show an alternating behavior, this is not always the case for ω. Among the exponents we have computed this is the case for ω corresponding to the O(2), O(3), and O(4) symmetric models. In those instances we did not apply Wynn's ϵ algorithm, and only cited our NNLO predictions as our final value for ω for the O(2), O(3), and O(4) symmetric models.

We use this method to accurately extrapolate to higher orders of the DE and thus obtain more precise predictions,

TABLE I. Our findings for the exponents of the Z_2 symmetric scalar model in $d = 3$ Euclidean dimensions (top four rows) for different orders of the DE and the improved, final prediction. The uncertainties are the sum of the uncertainties from the polynomial expansion and the regulator dependence. We compared these to some other methods: DE at NNLO (∂^4) with field expansion [13], at N^{3}LO (∂^6) without field expansion [11], MC [3], six-loop perturbation theory at fixed $d = 3$ [5], $d = 4 - \epsilon$ expansion at ϵ^6 [7], and the CB method [8].

Method	ν	η	ω
LPA	0.6504(7)	0	0.654(1)
NLO	0.629(5)	0.042(11)	0.84(4)
NNLO	0.6302(4)	0.0347(30)	0.820(10)
Improved	0.6301(4)	0.0358(30)	0.822(10)
∂^4, field exp.	0.632	0.033	
∂^6, no field exp.	0.63012(16)	0.0362(12)	0.832(14)
MC	0.63002(10)	0.03627(10)	0.832(6)
Six-loop PT	0.6304(13)	0.0335(25)	0.799(11)
ϵ^6, epsilon exp.	0.6292(5)	0.0362(6)	0.820(7)
CB	0.629971(4)	0.0362978(20)	0.82968(23)

since the functional space of Γ_k is less truncated at higher orders of the DE. Another systematic source of error is that of the DE itself. If one insists on using Wynn's epsilon algorithm, then it is necessary to compute the N^{3}LO prediction of the DE in order to give a conservative estimate on this error. In order to still give reliable predictions, we use the well-grounded error estimate for the DE proposed in Ref. [11] detailed in Appendix B.

V. PREDICTIONS FOR THE Z_2 SYMMETRIC SCALAR MODEL

We derived the β functions for the dimensionless scale-dependent functions $(U_k, Z_k, W_k, H_k, J_k)$ in the ansatz (5) using a *Mathematica* code. We verified the correctness of $\dot{U}_k$ and $\dot{Z}_k$ (at ∂^2 order) to be the same as in the literature [17,23]. We expanded these functions in the powers of the field yielding the β functions for the dimensionless couplings $\tilde{f}_n(k)$ in Eq. (19). We have calculated the effect of increasing M_F on the exponents. We start with the LPA, where the only scale-dependent function is U_k and locate the Wilson-Fisher fixed point with truncation threshold $M_U = 4$. In the next step, we locate the fixed point for $M_U = 5$ using the previous fixed-point solution with $\tilde{u}_5 = 1$ as initial value. After this, we move on to $M_U = 6$ using the previous fixed-point solution with $\tilde{u}_6 = 1$ as initial value. In this iterative manner, we find the Wilson-Fisher fixed point for up to $M_U = 8$. At the NLO, we have an additional scale-dependent function Z_k and nonzero anomalous dimension. We start with locating the fixed point at $M_U = 8$ and $M_Z = 0$, but including the effect of anomalous dimension and simply use the LPA values for $M_U = 8$ as initial value. Next, we apply to M_Z the iterative procedure used to find the fixed point for $M_U = 8$ at the LPA. We find the Wilson-Fisher fixed point for up to $M_U = 8$ and $M_Z = 8$. At NNLO, we have three scale-dependent functions W_k, H_k, and J_k. We start looking for the Wilson-Fisher fixed point at $M_U = M_Z = 8$ with $M_W = M_H = M_J = 0$, and setting the initial values to be $\tilde{w}_0 = \tilde{h}_0 = \tilde{j}_0 = 1$ for the new couplings. Finally, we also apply here the previously described iterative algorithm but we increase simultaneously M_W, M_H, and M_J and denote this value with M_{WHJ}. The upper limit where we have located the Wilson-Fisher fixed point is $M_{WHJ} = 7$.

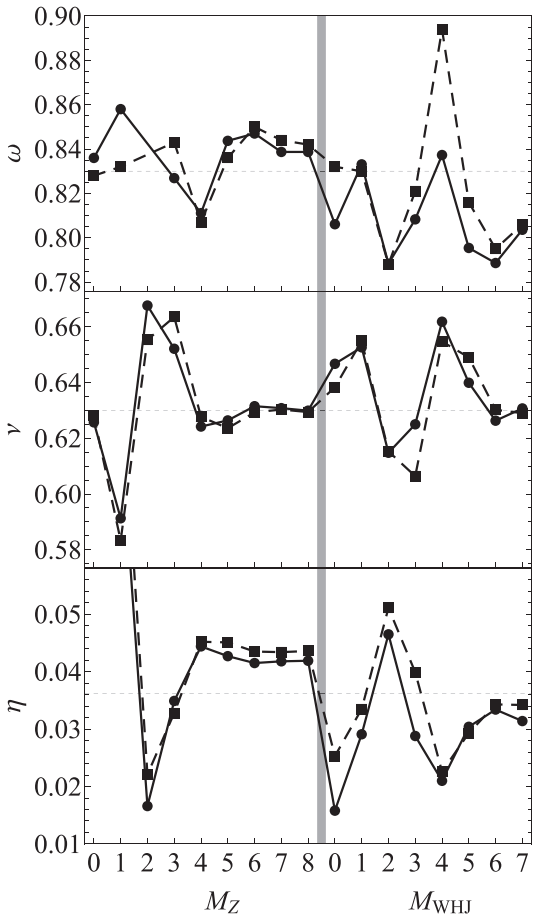

FIG. 1. The effect of the polynomial truncation in the Z_2 symmetric scalar model at NLO (left) and NNLO (right) on the critical exponents ν, η, and ω at $M_U = 8$. The continuous line with disks corresponds to the regulator r_Θ with $\alpha = 1/2$, the dashed line with squares to the regulator r_{exp} with $\alpha = 1$. The CB values are shown for reference with the dotted horizontal line.

We have computed the fixed points with the two regulators discussed in Sec. III. Using (13) with $\alpha = 1/2$ reduces the integrals (9) to linear combinations of the ${}_2F_1$ hypergeometric function, which greatly increases the speed of computations compared to (16) with any value of α.

The effect of the gradual inclusion of the new couplings can be seen in the left column of Fig. 1, which agrees with [13]. The most important conclusion is that while at ∂^2 order the contributions of the Taylor expansion in field variable become small for $M_Z > 4$, this threshold power value at ∂^4 order is somewhat larger, $M_{WHJ} = 6$. The magnitude of these contributions start to decrease monotonically for $M_Z > 3$ at NLO and $M_{WHJ} > 4$ at NNLO. Next, we apply the principle of minimal sensitivity to $M_{WHJ} \geqslant 4$, which corresponds to the last four data points in each row of Fig. 1. We have found that the optimal values α^{opt} for the regulators (13) and (16)

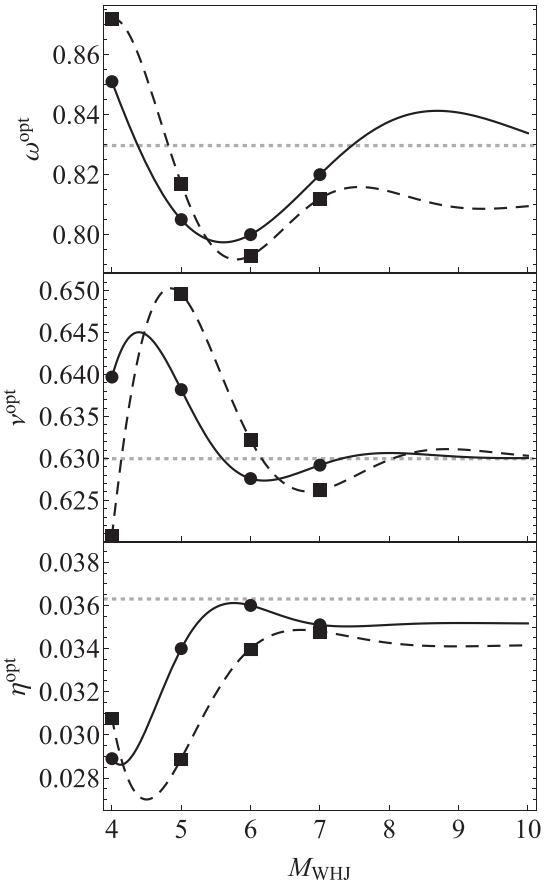

FIG. 2. A decaying function fit on the PMS optimized values of the exponents of the Z_2 symmetric scalar model at truncation $M_{WHJ} = 4$ and above. The disks correspond to the values obtained with r_Θ, and the squares to the values obtained with $r_{\rm exp}$. The dashed horizontal line shows the CB values.

exhibit only small fluctuations around $\alpha^{\rm opt} = 0.35$ and 0.8 for $M_{WHJ} = 0, \ldots, 7$. The only instance for which we have not found a PMS solution is for the truncation $M_{WHJ} = 0$. The explicit values for the optimal parameter value $\alpha^{\rm opt}$ corresponding to $M_{WHJ} = 7$ are found to be $\alpha^{\rm opt} = 0.30$ for the regulator (13) and $\alpha^{\rm opt} = 0.76$ for (16). Once we acquire the optimized results in this asymptotic regime, where each successive contribution from the Taylor expansion is smaller than the previous one, we fit a decaying and alternating function to these data points in an attempt to capture the behavior of the Taylor series and resum the corrections from the Taylor expansion. The model function in every instance is

$$X(M) = a + be^{-cM}\sin(dM + e), \tag{22}$$

with the independent variable being M the degree of polynomial truncation and the fitted parameters are a, b, d, e, and $c > 0$. This step is shown in Fig. 2. We consider our findings to be the $M_{WHJ} \to \infty$ limit of these fitted functions; that is, we identify the exponent as $X(M \to \infty) = a$ from the model function (22). We do not apply Wynn's epsilon algorithm here, because the corrections from increasing M_{WHJ} is not a simple alternating series. In the asymptotic regime, however, shown with the PMS optimized exponent in Fig. 2, these corrections alternate around their limiting value with periodicity of at least two. For instance, we expect that the correction from $M_{WHJ} = 8$ increases the value of $\nu^{\rm opt}$ compared to $M_{WHJ} = 7$ and the higher corrections to have a smaller effect than this. The model function (22) takes this into account correctly.

Every β function contains terms proportional to η through $\dot{R}_k$. Considering only the exponents ν and η, the inclusion of these terms in $\dot{\tilde{U}}_k$ gives a 1% and 5% correction, while in $\dot{\tilde{Z}}_k$ they give a 0.1% and 0.5% correction compared to not including those. We have also inspected the inclusion of these terms into $\dot{\tilde{W}}_k$, $\dot{\tilde{H}}_k$, and $\dot{\tilde{J}}_k$ for the truncation $M_U = 8$ and $M_Z = 8$ with $M_{WHJ} \leqslant 4$ and found that this characteristically gives a 0.02% and 0.008% correction to the exponents. We have neglected this correction in $\dot{\tilde{W}}_k$, $\dot{\tilde{H}}_k$, and $\dot{\tilde{J}}_k$ for $M_{WHJ} \geqslant 5$ and considered it as one source of uncertainty. The other source comes from the truncation of $\tilde{U}_k$ and $\tilde{Z}_k$. As a double check, we have computed the fixed point for truncation $M_U = 9$, $M_Z = 8$ and $M_U = 9$, $M_Z = 9$ at NLO. We have found that the inclusion of the coupling $\tilde{u}_9$ has negligible effect compared to the inclusion of $\tilde{z}_9$. Our final predictions for the critical exponents of the Z_2 symmetric model are shown in Table I. The method to obtain the predictions and their corresponding uncertainty are detailed in Appendix B.

VI. NNLO FOR THE O(N) SYMMETRIC SCALAR MODELS

A. Modifications compared to the Z_2 symmetric case

There are more scale-dependent functions in the O(N) symmetric scalar model beyond the LPA than in the Z_2 symmetric one, due to an additional group index. At NLO, there are two instead of the one Z_k, but at NNLO the number of independent scale-dependent functions increases to ten, compared to the three W_k, H_k, and J_k. The complete ∂^4-order ansatz is

$$\begin{aligned}\Gamma_k[\vec{\phi}] = \int_x \Big\{ & U_k + \frac{1}{2}Z_k(\partial\phi_x^a)^2 + \frac{1}{4}Y_k(\partial\rho_x)^2 + \frac{1}{2}W_{1,k}\big(\partial_\mu\partial_\nu\phi_x^a\big)^2 + \frac{1}{4}W_{2,k}\big(\phi_x^a\partial_\mu\partial_\nu\phi_x^a\big)^2 + \frac{1}{2}H_{1,k}\big(\partial\phi_x^a\big)^2\big(\phi_x^b\partial^2\phi_x^b\big) \\ & + H_{2,k}(\partial_\mu\rho_x)\big(\partial^\mu\phi_x^b\big)\big(\partial^2\phi_x^b\big) + \frac{1}{4}H_{3,k}\big(\partial\rho_x\big)^2\big(\phi_x^a\partial^2\phi_x^a\big) + \frac{1}{8}J_{5,k}\big(\partial\rho_x\big)^4 + \frac{1}{2}J_{1,k}\big(\partial\phi_x^a\big)^2\big(\partial\phi_x^b\big)^2 \\ & + \frac{1}{2}J_{2,k}\big(\partial_\mu\phi_x^a\big)\big(\partial_\nu\phi_x^a\big)\big(\partial^\mu\phi_x^b\big)\big(\partial^\nu\phi_x^b\big) + \frac{1}{4}J_{3,k}\big(\partial\rho_x\big)^2\big(\partial\phi_x^a\big)^2 + \frac{1}{4}J_{4,k}\big(\partial_\mu\rho_x\big)\big(\partial_\nu\rho_x\big)\big(\partial^\mu\phi_x^b\big)\big(\partial^\nu\phi_x^b\big)\Big\},\end{aligned} \tag{23}$$

where $\vec{\phi}$ is the N component scalar field and $\rho_x = \phi_x^a \phi_x^a/2$ is the invariant under the O(N) symmetry transformation. We have suppressed the field dependence of the scale-dependent functions in (23) to be more transparent. Due to the appearance of the Goldstone modes in addition to the one massive mode in the Z_2 symmetric model, we have two anomalous dimensions corresponding to these modes:

$$\eta = -k\partial_k \ln Z_k(\rho^*), \tag{24}$$

$$\tilde{\eta} = -k\partial_k \ln(Z_k(\rho^*) + \rho^* Y_k(\rho^*)) \equiv -k\partial_k \ln \tilde{Z}_k(\rho^*). \tag{25}$$

These anomalous dimensions are equal in the critical point. In our numerical check, we use this fact to ensure the correctness of our equations. Besides the field, the regulator function also receives O(N) indices. We choose

$$R_k^{ab}(y) = \delta^{ab} Z_k(\rho^*) k^2 y\, r(y), \tag{26}$$

where δ^{ab} is the Kronecker-delta matrix, such that the regulator mass matrix is already diagonalized in the O(N) space. In order to facilitate the bookkeeping of the O(N) indices, we introduce projectors P_A^{ab} with ($A = \parallel, \perp$) to the radial ($P_\parallel^{ab} = e^a e^b$) and perpendicular (Goldstone) ($P_\perp^{ab} = \delta^{ab} - e^a e^b$) directions in the O($N$) space, with e^a being the unit vector. The scale-dependent functions Y_k, $W_{i,k}$, $H_{i,k}$, and $J_{i,k}$ are obtained by the same momentum derivatives [Eq. (6)] as Z_k, W_k, H_k, and J_k in the Z_2 symmetric model as coefficients of the integrands in $\int_{Q_1,\ldots,Q_n} \prod_{i=1}^n \eta_{Q_i}^{A_i} \delta(\sum_{i=1}^n Q_i)$. The capital Latin letters correspond to either $\parallel$ or ($\perp, a$). Using the projectors defined above one has

$$P_\parallel^{ab} \eta_x^a = \eta_x^\parallel \quad \text{and} \quad P_\perp^{ab} \eta_x^a = \eta_x^{\perp,a}. \tag{27}$$

In this method, every O(N) index is contracted in the final result, so that $\eta_Q^{\perp,a}$ may occur only in pairs, such as $\eta_Q^{\perp,a}\eta_{-Q}^{\perp,a}$. For instance, the left-hand side of the Wetterich equation for $\mathcal{O}(\eta^2)$ Eq. (3) modifies to

$$\int_Q \eta_Q^{\perp,a}\eta_{-Q}^{\perp,a}(\dot{Z}_k Q^2 + \dot{W}_{1,k} Q^4 + \dot{U}') + \int_Q \eta_Q^{\parallel}\eta_{-Q}^{\parallel}((\dot{Z}_k + \dot{Y}_k)Q^2 + (\dot{W}_{1,k} + \dot{W}_{2,k})Q^4 + \dot{U}' + 2\rho\dot{U}'') \tag{28}$$

with the ansatz in Eq. (23).

We have followed the same steps of numerical analysis as we did for the Z_2 symmetric model. The system of β functions is generated by a *Mathematica* code, which is then verified to reproduce the ∂^2-order results [24]. We applied the same iterative algorithm to find the Wilson-Fisher fixed point for high values of truncation M as for the Z_2 symmetric model. At the LPA, we have computed the exponents for up to $M_U = 8$. In the NLO we have increased simultaneously the truncation M_Z of Z_k and M_Y of Y_k for up to $M_Z = M_Y = 5$ and denote this with M_{ZY}. At NNLO, we have ten scale-dependent functions. In order to make it easier to find the Wilson-Fisher fixed point, we further divide the iterative algorithm into three parts. First, we locate the fixed point for the truncation $M_U = 8, M_{ZY} = 5$, $M_{W_1} = M_{W_2} = 0$ with the initial values $\tilde{w}_{1,0} = \tilde{w}_{2,0} = 1$. In the next step, we use this fixed point as initial value with $\tilde{h}_{1,0} = \tilde{h}_{2,0} = \tilde{h}_{3,0} = 1$ for the truncation $M_U = 8$, $M_{ZY} = 5$, $M_{W_1} = M_{W_2} = 0$, and $M_{H_1} = M_{H_2} = M_{H_3} = 0$. In the last step we locate the fixed point with $M_{J_i} = 0$ ($i = 1, \ldots, 5$) also included. We denote this truncation with $M_{WHJ} = 0$ when all the NNLO level scale-dependent functions are included with zeroth-order truncation in their Taylor expansion. We have computed the exponents for up to $M_U = 8$, $M_{ZY} = 5$, and $M_{WHJ} = 4$.

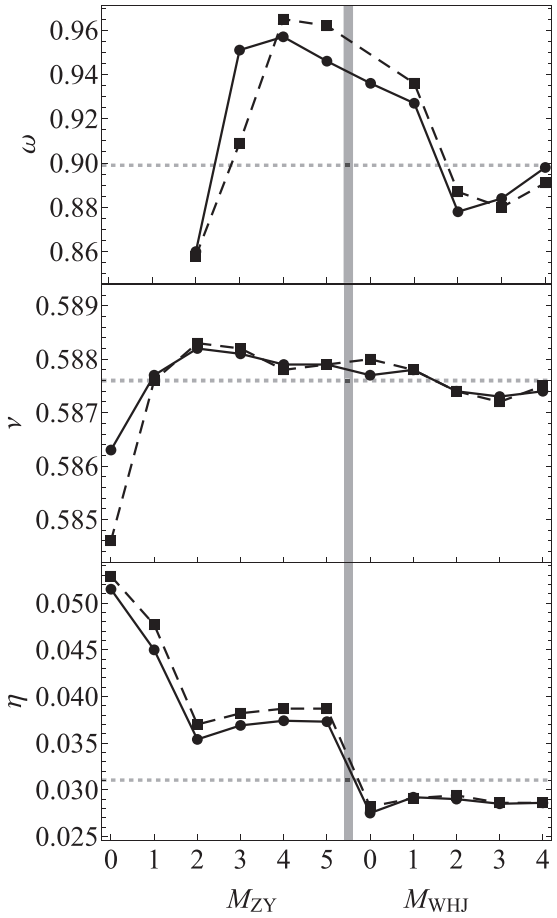

FIG. 3. The dependence of the critical exponents ν, η, and ω on the order of polynomial truncation for the O(0) symmetric model at $M_U = 8$. The vertical line separates our NLO results (left) from the NNLO ones (right). The dotted horizontal line shows the corresponding MC result. The continuous curve with disk markers belongs to the Θ-type regulator (13) with $\alpha = 1/2$, while the dashed curve with rectangle markers belongs to the exponential-type regulator (16) with $\alpha = 1$. At the points, where ω is not shown, it is a complex number.

B. Numerical findings

We have computed the critical exponents for the regulators (13) and (16). The former one with $\alpha = 1/2$ reduces a large number of the threshold integrals to ${}_2F_1$-type hypergeometric functions. This yields a significant speed boost in the computations compared to (16) with any value of α.

The effect of the gradual inclusion of the new couplings for the O(N) symmetric scalar model is shown in Figs. 3–7 for $N = 0$–4. We have also computed the exponents for the $N = 10$ and $N = 100$ cases but omitted to show their field dependence, as it is very small. The leading order of the DE,

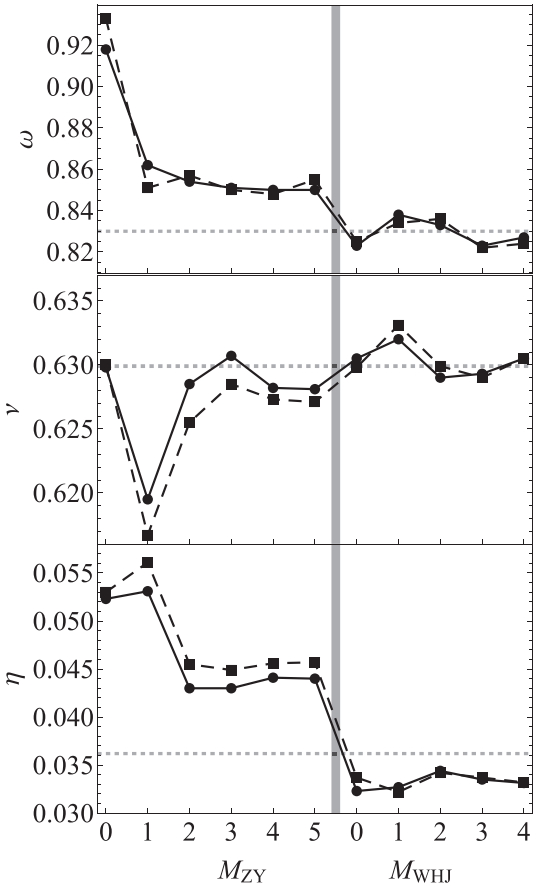

FIG. 4. The dependence of the critical exponents ν, η, and ω on the order of polynomial truncation for the O(1) symmetric model at $M_U = 8$. The vertical line separates our NLO results (left) from the NNLO ones (right). The dotted horizontal line shows the corresponding CB result. The continuous curve with disk markers belongs to the Θ-type regulator (13) with $\alpha = 1/2$, while the dashed curve with rectangle markers belongs to the exponential-type regulator (16) with $\alpha = 1$.

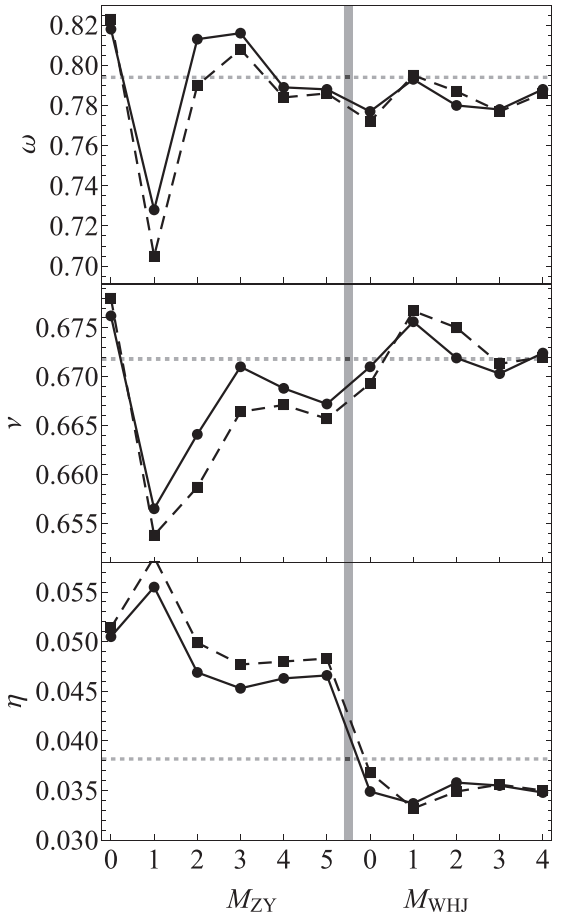

FIG. 5. The dependence of the critical exponents ν, η, and ω on the order of polynomial truncation for the O(2) symmetric model at $M_U = 8$. The vertical line separates our NLO results (left) from the NNLO ones (right). The dotted horizontal line shows the corresponding CB result. The continuous curve with disk markers belongs to the Θ-type regulator (13) with $\alpha = 1/2$, while the dashed curve with rectangle markers belongs to the exponential-type regulator (16) with $\alpha = 1$.

the LPA is exact for $O(N \to \infty)$. The anomalous dimension decreases monotonically at large N values with increasing N and vanishes completely in the limit $N \to \infty$. This means that the derivative expansion has to yield very precise predictions for the exponents for large N values. This is reflected in the fact that the field dependence is very small at $N = 10$ and at $N = 100$. We have chosen $N = 10$ and 100 as benchmark points to compare our predictions with those of the large-N expansion. We also show the field dependence of the O(1) symmetric model, which should give the critical exponents for the Z_2 universality class. This feature is nicely shown in Fig. 4. Going back to Figs. 3–7, we can clearly see that the field expansion is very stable at NNLO even when one considers the correction of $M_{WHJ} = 1$ compared to $M_{WHJ} = 0$. Due to this smoothness of predictions from the field expansion at NNLO, we apply the principle of minimal sensitivity for $M_{WHJ} \geqslant 0$. In order to reduce the amount of computation, we have only looked for a PMS solution for the anomalous dimension and accepted the corresponding parameter value as the optimal $\alpha^{\rm opt}$. We have found that $\alpha^{\rm opt}$ depends weakly both on the truncation M_{WHJ} and on the O(N) model considered. We have found at NNLO with truncation $M_{WHJ} = 4$ for the regulator (13) that $\alpha^{\rm opt} = 0.340(10)$ while for (16) we have obtained $\alpha^{\rm opt} = 0.87(1)$. The uncertainty corresponds to the dependence of $\alpha^{\rm opt}$ on the specific O(N) model considered. For instance, we obtained $\alpha^{\rm opt} = 0.337$ for the regulator (13) in the case of the O(0) model with truncation $M_{WHJ} = 4$ and $\alpha^{\rm opt} = 0.344$ in the case of the O(3) model in the same setting. We attempt to find the limiting value of the optimized exponents corresponding to $M_{WHJ} = 0, \ldots, 4$ in the range $N = 0$–4 for $M_{WHJ} \to \infty$ in the same fashion as we did for the Z_2 symmetric model (see Fig. 2). We have also checked the stability of the predictions from (22). We have computed the extrapolated values of the critical exponents from (22) by fitting those to the PMS optimized exponents corresponding to $M_{WHJ} = 0, \ldots, 4$ and $M_{WHJ} = 0, \ldots, 3$. In the latter case we also incorporated an assumption for the fit. Namely, whether we expect (from the trend of the polynomial expansion) $X(M_{WHJ} = 4)$ to be greater or smaller than $X(M_{WHJ} = 3)$. As a result we obtained that the difference between the predictions obtained from the fits are two to three

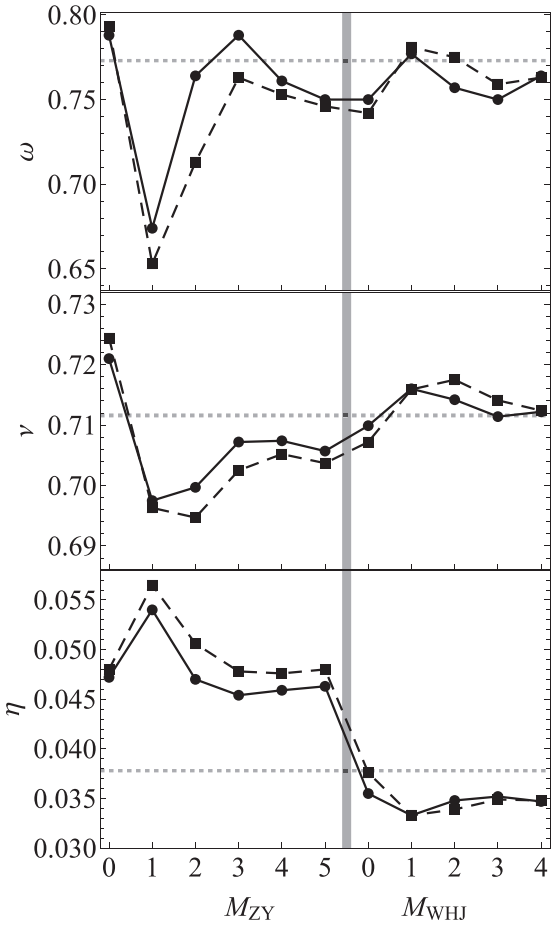

FIG. 6. The dependence of the critical exponents ν, η, and ω on the order of polynomial truncation for the O(3) symmetric model at $M_U = 8$. The vertical line separates our NLO results (left) from the NNLO ones (right). The dotted horizontal line shows the corresponding MC result. The continuous curve with disk markers belongs to the Θ-type regulator (13) with $\alpha = 1/2$, while the dashed curve with rectangle markers belongs to the exponential-type regulator (16) with $\alpha = 1$.

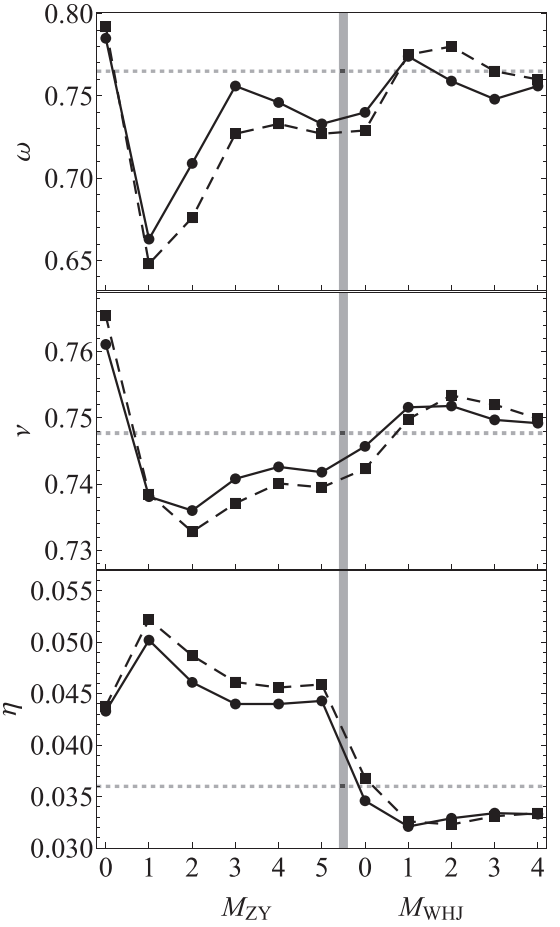

FIG. 7. The dependence of the critical exponents ν, η, and ω on the order of polynomial truncation for the O(4) symmetric model at $M_U = 8$. The vertical line separates our NLO results (left) from the NNLO ones (right). The dotted horizontal line shows the MC bootstrap result. The continuous curve with disk markers belongs to the Θ-type regulator (13) with $\alpha = 1/2$, while the dashed curve with rectangle markers belongs to the exponential-type regulator (16) with $\alpha = 1$.

times smaller than the difference between the raw values corresponding to $M_{WHJ} = 4$ and $M_{WHJ} = 3$. This is the method to obtain the uncertainty $\Delta_{\text{poly}}\overline{X}^{(4)}$ detailed in Appendix B. As for $N = 10$ and $N = 100$, the fluctuation of the exponents is very small with varying M_{WHJ}. In these instances we consider our final predictions corresponding to $M_{WHJ} = 3$ and $M_{WHJ} = 2$, respectively, with PMS optimization applied.

Considering the above discussed details, our predictions for O(N) critical exponents at fixed orders of the DE are summarized in Table II. Our findings at the level of LPA correspond to the exponents computed at $M_U = 8$ with the method detailed at the end of Sec. III C. We obtain that the optimal value $\alpha^{\text{opt}}_{\text{LPA}}$ of the parameter α is 0.9 for (13) and 5 for (16) at LPA. Going further, our NLO findings are computed at $M_U = 8$ and $M_{ZY} = 5$ with $\alpha^{\text{opt}}_{\text{NLO}} = 0.4$ and 1.4 for (13) and (16), respectively. The results for the NNLO level results are discussed above. The method we used to compute the central values and the uncertainties is detailed in Appendix B.

VII. BRIEF SUMMARY OF THE O(N) CRITICAL EXPONENTS FROM VARIOUS METHODS

The O(N) symmetric scalar model was first introduced as the n-vector model as a generalization of some physically relevant models [38] in d Euclidean dimensions. The $N = 0$ case describes the self-avoiding walk [39,40]. It is also noteworthy that the O(0) model probably does not have a Minkowskian counterpart, because in the case in which the Euclidean dimension d and N are not positive integers the unitarity of the corresponding Minkowskian model is lost or at least highly nontrivial. At the level of the n-vector model, the O(1) model describes the Ising universality class. In the ERG, however, the Z_2 and O(N) symmetric models at $N = 1$ seem to be different because of the different content of scale-dependent functions and the appearance of an additional, massless excitation in the O(N) model. The two models are equivalent, however. The flow equations for the O(N) model in the limit of $N \to 1$ are regular. Furthermore the contribution of the Goldstone modes in the flow equations vanish for $N = 1$,

TABLE II. The main findings of this work. Our predictions for the critical exponents ν, η, and ω at the LPA, NLO, and NNLO of the DE for the O(N) symmetric models in $d = 3$ Euclidean dimensions. These values are the average of the PMS optimized predictions, computed from the Θ regulator (13) and the exponential regulator (16) and the deviation from the average is one source of the uncertainties. The other source of uncertainty corresponds to the polynomial truncation of the scale-dependent functions.

N	Order of DE	ν	η	ω
0	LPA	0.5924(3)	0	0.656(2)
	NLO	0.588(1)	0.038(9)	0.95(8)
	NNLO	0.5876(1)	0.030(3)	0.894(16)
1	LPA	0.6504(7)	0	0.654(1)
	NLO	0.628(6)	0.045(11)	0.85(5)
	NNLO	0.630(1)	0.035(3)	0.829(6)
2	LPA	0.7098(10)	0	0.672(1)
	NLO	0.667(10)	0.047(13)	0.79(3)
	NNLO	0.673(2)	0.036(3)	0.784(8)
3	LPA	0.7629(12)	0	0.702(1)
	NLO	0.705(15)	0.047(13)	0.75(3)
	NNLO	0.713(3)	0.036(3)	0.765(3)
4	LPA	0.8060(12)	0	0.737(2)
	NLO	0.741(20)	0.045(13)	0.73(3)
	NNLO	0.749(3)	0.034(3)	0.763(9)
10	LPA	0.9193(5)	0	0.874(2)
	NLO	0.878(10)	0.027(7)	0.79(2)
	NNLO	0.877(1)	0.022(2)	0.810(7)
100	LPA	0.9925(1)	0	0.9881(2)
	NLO	0.989(1)	0.0030(7)	0.978(3)
	NNLO	0.9888(3)	0.00264(8)	0.9780(6)

and the extra flow equations decouple from those which have direct interpretation in terms of the Z_2 symmetric model. The O(2) model is more commonly known as the XY model, which is used to describe the phase transition in the superfluid helium-4. The O(3) model is also known as the Heisenberg model for ferromagnetism. Last but not the least, the O(4) model can be considered as a toy model for the standard model's Higgs sector, but also applicable to chiral phase transitions.

Some of the most precise computations of the O(N) critical exponents in $d = 3$ Euclidean dimensions are summarized in Table III. Comparing these with our findings, "This work" entry in the same table, one can see that the central values are in excellent agreement. The improved results of Ref. [11] take advantage of the convergence of the DE as well as the alternating behavior of the corrections from the successive orders of the DE. In contrast, our improvement, the Wynn epsilon algorithm detailed in Sec. IV, is a robust series acceleration method applicable to any alternating sequence.

VIII. CONCLUSION

We have computed the critical exponents for the Z_2 and O(N) symmetric scalar models in $d = 3$ Euclidean dimensions. We have employed the exact renormalization group equation for the effective average action. We have used the derivative expansion at NNLO (or ∂^4 order) and calculated

TABLE III. Critical exponents of the O(N) symmetric scalar model in $d = 3$ Euclidean dimensions for several N values with different methods: our improved predictions using Wynn's epsilon algorithm, the DE at NNLO (∂^4) without field expansion with raw (computed with the exponential regulator) and improved values [11], Monte Carlo simulations, six-loop perturbation theory at fixed $d = 3$ [5], $d = 4 - \epsilon$ expansion at ϵ^6 [7], the conformal bootstrap method, and the large-N expansion [35–37].

N	Method	ν	η	ω
0	This work	0.5875(1)	0.031(3)	0.903(16)
	∂^4, raw	0.5875	0.0292	0.901
	∂^4, improved	0.5876(2)	0.0312(9)	0.901(24)
	MC [25,26]	0.58759700(40)	0.0310434(30)	0.899(14)
	Six-loop PT	0.5882(11)	0.0284(25)	0.812(16)
	ϵ^6, ϵ-exp.	0.5874(3)	0.0310(7)	0.841(13)
	CB [27]	0.5876(12)	0.0282(4)	
2	This work	0.672(2)	0.038(3)	0.784(8)
	∂^4, raw	0.6732	0.0350	0.793
	∂^4, improved	0.6716(6)	0.0380(13)	0.791(8)
	MC [4]	0.67169(7)	0.03810(8)	0.789(4)
	Six-loop PT	0.6703(15)	0.0354(25)	0.789(11)
	ϵ^6, ϵ-exp.	0.6690(10)	0.0380(6)	0.804(3)
	CB [28]	0.6718(1)	0.03818(4)	0.794(8)
3	This work	0.712(3)	0.038(3)	0.765(3)
	∂^4, raw	0.7136	0.0347	0.773
	∂^4, improved	0.7114(9)	0.0376(13)	0.769(11)
	MC [29,30]	0.7116(10)	0.0378(3)	0.773
	Six-loop PT	0.7073(35)	0.0355(25)	0.782(13)
	ϵ^6, ϵ-exp.	0.7059(20)	0.0378(5)	0.795(7)
	CB [31,32]	0.7120(23)	0.0385(13)	0.791(22)
4	This work	0.748(3)	0.036(3)	0.763(9)
	∂^4, raw	0.7500	0.0332	0.765
	∂^4, improved	0.7478(9)	0.0360(12)	0.761(12)
	MC [30,33]	0.7477(8)	0.0360(4)	0.765
	Six-loop PT	0.741(6)	0.0350(45)	0.774(20)
	ϵ^6, ϵ-exp.	0.7397(35)	0.0366(4)	0.794(9)
	CB [32,34]	0.7472(87)	0.0378(32)	0.817(30)
10	This work	0.877(1)	0.023(2)	0.805(7)
	∂^4, raw	0.8771	0.0218	0.808
	∂^4, improved	0.8776(10)	0.0231(6)	0.807(7)
	Large-N	0.87(2)	0.023(2)	0.77(1)
100	This work	0.9887(3)	0.00267(8)	0.9780(6)
	∂^4, raw	0.98877	0.00260	0.977
	∂^4, improved	0.9888(2)	0.00268(4)	0.9770(8)
	Large-N	0.9890(2)	0.002681(1)	0.9782(2)

the β functions for the scale-dependent functions, shown in (5) for the Z_2 and in (23) for the O(N) symmetric models. In order to locate the Wilson-Fisher fixed point which is the nontrivial fixed-point solution of the β functions, we have expanded the scale-dependent functions in powers of the field. We interpret the scale-dependent coefficients $f_n(k)$ from the Taylor expansion as effective coupling strengths for the interaction vertices of the field they multiply. We have located the fixed point in the theory space spanned by the (canonical mass) dimensionless couplings, with truncated Taylor series of the scale-dependent functions. Our main findings for the Z_2 symmetric model shown in Table I are in agreement with predictions obtained using other methods. We have used the

Z_2 symmetric model as a testing ground for the correctness of our *Mathematica* code. We then generalized this code for the O(N) symmetric model and computed the critical exponents for some relevant N values. We have tested the O(N) *Mathematica* code for the $N = 1$, 10, and 100 cases. The first benchmark point $N = 1$ is chosen, because it should reproduce the Ising critical exponents as the O(1) and Z_2 symmetric models are equivalent as discussed in Sec. VII. We chose $N = 10,\ 100$ to be second and third benchmark points, because the effect of the derivative expansion is diminished with $N \to \infty$, hence it can give very accurate results for large N values. Our main findings are summarized in Table II. A great advantage of the computations employed in this work is that they require noticeably less computer time than most of the other methods. For our highest employed polynomial truncation both for the Z_2 and O(N) symmetric models, the location of the Wilson-Fisher fixed point roughly takes 1–2 h, while computing the Jacobian matrix at the fixed point takes an additional hour on a single desktop PC.

In a recent paper [11] the authors have performed similar computations with the ERG. The differences are that (i) we have not truncated our formulas in the momenta (denoted here with Q_i); (ii) we have employed Taylor expansion for the scale-dependent functions in powers of the field instead of shooting for a solution for the complete scale-dependent functions; and (iii) we have computed the exponents with the regulator (13), which is the simplest regulator at NNLO. Although this Θ regulator is argued to perform poorly in [10], we have found that it yields excellent predictions for the exponents in the models studied here. We also provide improved predictions using Wynn's epsilon algorithm on our predictions of the DE, yielding central values which are in excellent agreement with other precise methods used to compute critical exponents.

We also produce the subleading scaling corrections ω_i (from the eigenvalue spectrum $-1/\nu < \omega < \omega_1 < \omega_2 < \ldots$ of the Jacobian of the β functions) as a by-product of computing the exponents ν and ω. The expansion of the scale-dependent functions in powers of the field is also applicable to explore the phase structure of a model and the RG running of its couplings. The derivative expansion can also be improved to N^{3}LO (or ∂^6 order) with some effort for the O(N) symmetric models, which would provide more precise exponent values for many cases of N.

ACKNOWLEDGMENT

The author would like to thank Z. Trócsányi for the careful reading of the manuscript.

APPENDIX A: THE THETA REGULATOR AS A LIMIT OF A CONTINUOUS REGULATOR

Regulators, which are not C^∞ functions, are not applicable beyond a certain order in the DE. Some threshold integrals at the NNLO of the DE evaluated with (13) are ambiguous, or even undefined [41] when $\delta(0)$ appears after performing the integration of the threshold functions. The purpose of this Appendix is to prove that the ambiguity of the threshold integrals is lifted when one considers (13) as the limit of a C^∞-type regulator. We consider

$$r_\beta(y) = \alpha \frac{(1-y)^2}{y} \frac{1}{1+e^{-2\beta(1-y)}}, \tag{A1}$$

with the property

$$\lim_{\beta\to\infty} r_\beta(y) = r_\Theta(y). \tag{A2}$$

Actually, the only ambiguous integral with (13) is of type $M^{d,4}_{m,1}$. Thus we are going to compute this integral with (A1) and prove that in the $\beta \to \infty$ limit we unambiguously recover the result in Eq. (15). It is convenient to introduce the integration variable $\epsilon = y - 1$ and to compute explicitly the derivatives of (A1), resulting in

$$M^{d,4}_{m,1} = -128\alpha^2\left(Z_k^2 k^{d+2}\right)\frac{\Omega_d}{(2\pi)^d} I_\beta, \tag{A3}$$

where

$$I_\beta = \int_{-1}^{\infty} d\epsilon \frac{(1+\epsilon)^{-1+d/2}}{\left[\omega + (1+\epsilon)Z + (1+\epsilon)^2 W + \alpha\frac{\epsilon^2}{1+e^{2\beta\epsilon}}\right]^m} \times \epsilon\mathcal{I}. \tag{A4}$$

Here we organized all the derivatives of the regulator into the function $\mathcal{I}$:

$$\mathcal{I} = \beta^2 \frac{e^{6\beta\epsilon}}{(1+e^{2\beta\epsilon})^7}\{\beta\epsilon(\epsilon+1)\sinh(\beta\epsilon) + [\epsilon(\beta\epsilon+\beta-1)-2]\cosh(\beta\epsilon)\}\left([3\sinh(\beta\epsilon)+\sinh(3\beta\epsilon)]\right.$$
$$\left. + \beta\epsilon\{\beta\epsilon[\sinh(3\beta\epsilon) - 11\sinh(\beta\epsilon)] + 12\cosh(\beta\epsilon) - 4\cosh(3\beta\epsilon)\}\right). \tag{A5}$$

We have also written the inverse propagator G explicitly and ω, Z, and W correspond to the scale-dependent functions $2\rho U_k''(\rho)$, $Z_k(\rho)$, and $W_k(\rho)$. If one considers the integral I_β as the sum of three integration regions

$$\int_{-1}^{-a} + \int_{-a}^{a} + \int_{a}^{\infty} \tag{A6}$$

with $0 < a \ll 1$, then in the limit $\beta \to \infty$, the integrands of the integrals over the regions $[-1, -a]$ and $[a, \infty)$ vanish. Hence, in our computations we need the limit

$$\lim_{\beta\to\infty} I_\beta = \lim_{\beta\to\infty} I_\beta(a), \tag{A7}$$

where

$$I_\beta(a) = \int_{-a}^{a} d\epsilon \frac{(1+\epsilon)^{-1+d/2}}{\left[\omega + (1+\epsilon)Z + (1+\epsilon)^2 W + \alpha\frac{\epsilon^2}{1+e^{2\beta\epsilon}}\right]^m} \times \epsilon\mathcal{I}, \tag{A8}$$

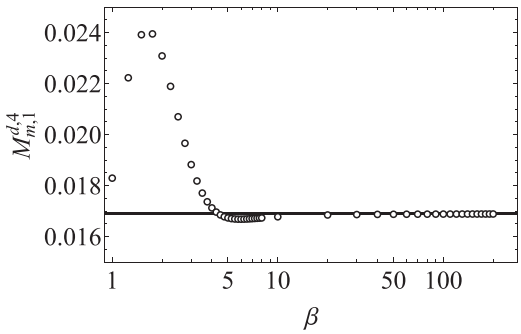

FIG. 8. The threshold function $M^{d,4}_{m,1}$ evaluated by numerical integration of the integral (A4) (open circles) at different values of β versus the analytical result (corresponding to $\beta \to \infty$) shown in Eq. (15) (straight line). We considered dimensionless variables and set $d = 3, \alpha = \tilde{\omega} = \tilde{Z} = \tilde{W} = 1$ for the sake of example.

with a being a small positive integer, so we can expand the dimension-dependent and inverse propagator part of $I_\beta(a)$ in Taylor series. At leading order (LO), this Taylor expansion leads to

$$I^{\rm LO}_\beta(a) = \frac{1}{(\omega + Z + W)^m} \int_{-a}^{a} d\epsilon\, \epsilon \mathcal{I} \equiv \frac{1}{G(1)^m} \int_{-a}^{a} d\epsilon\, \epsilon \mathcal{I}. \tag{A9}$$

This integral can be computed analytically and results in a very long combination of polynomials of β, ϵ, and polylogarithms; we do not show the explicit result here as it can be verified with the integrator of *Mathematica*, for instance. Now, we are in the position to take the limit $\beta \to \infty$ of the integral, which is independent of a,

$$I^{\rm LO}_{\beta\to\infty} = -\frac{1}{32} \frac{1}{(\omega + Z + W)^m}. \tag{A10}$$

One can, of course, take into account higher-order terms in the Taylor expansion of the dimension-dependent and inverse propagator part of (A8) so that the nth-order term in this expansion will be proportional to

$$\int_{-a}^{a} d\epsilon^{1+n} \epsilon \mathcal{I}. \tag{A11}$$

Such higher-order terms vanish in the limit $\beta \to \infty$, which we show here for the NLO approximation—also independent of a—to (A8),

$$I^{\rm NLO}_\beta = -\frac{1}{32} \frac{1}{G(1)^m} \left[1 + \left(\frac{1}{\beta} \frac{7\pi^4 - 360}{1200} \right) \times \left(\frac{d}{2} - 1 - m \frac{1 + 2W}{G(1)} \right) + \mathcal{O}\left(\frac{1}{\beta^3} \right) \right]. \tag{A12}$$

As the final result in the $\beta \to \infty$ limit we obtain

$$M^{d,4}_{m,1} = 4\alpha^2 \left(Z_k^2 k^{d+2} \right) \frac{\Omega_d}{(2\pi)^d} \frac{1}{G(1)^m}, \tag{A13}$$

which coincides with (15). We conclude that the regulator is unambiguous at the NNLO of the DE once considered as the limit of a C^∞-type regulator. A numerical example is also shown in Fig. 8. We have claimed in the main text, that with the regulator (13)

$$M^{d,3}_{m,1} = 0, \tag{A14}$$

due to the properties of the Dirac delta. Here we show that this integral with the regulator (A1) indeed vanishes in the limit $\beta \to \infty$. Using an identical derivation as used for $M^{d,4}_{m,1}$ above, it is straightforward to show that

$$M^{d,3}_{m,1} = \lim_{\beta\to\infty} \left(-\alpha^2 \left(Z_k^2 k^{d+2} \right) \frac{\Omega_d}{(2\pi)^d} \frac{1}{G(1)^m} \right) \times \left[\left(\frac{7\pi^4 - 360}{450\beta} \right) + \mathcal{O}\left(\frac{1}{\beta^3} \right) \right]. \tag{A15}$$

As a check, one can compute numerically the integral $M^{d,3}_{m,1}$ for arbitrary values of β using the regulator (A1) and compare it to the analytical result in Eq. (A15). Using the numerical integrations similar to those used for Fig. 8, we obtain -1.5100×10^{-5} from the direct numerical integration and -1.5098×10^{-5} from the analytical result (A15) at $\beta = 200$. The integrands of $M^{d,2}_{m,1}$ and $M^{d,1}_{m,1}$ using the regulator (A1) unambiguously reduce to those corresponding to the Θ regulator (13) in the limit $\beta \to \infty$. This is also the case for the threshold integrals $N^{d+a,\beta,\gamma}_{m,b,c}$, when β and γ are 1 or 2. If either β or γ is 3, then the integral behaves as $M^{d,3}_{m,1}$, which we have already discussed.

APPENDIX B: THE ERROR ESTIMATES AND CENTRAL VALUES

In this work we follow the instructions of Ref. [11] for appropriate error bars. However, due to the polynomial expansion an additional source of error appears. We summarize here the steps we take in this work to obtain the final prediction for the exponent X and also to obtain its uncertainty. First, at a given order (∂^s) of the DE we compute the PMS optimized value for various order M of the polynomial truncation of the scale-dependent functions (where M belongs to the least truncated case) for the regulators (13) and (16). This way we obtain the set of raw data $\{X^{(s),\rm opt}_{M,\Theta}, X^{(s),\rm opt}_{M,\rm exp}\}$. Let us now discuss the computation of the final values and the different sources of uncertainties considered in this work point by point.

(i) One can choose for the final result $\overline{X}^{(s)}$ at a given order of the DE the central value $\overline{X}^{(s)} \equiv \overline{X}^{(s)}_M = (X^{(s),\rm opt}_{M,\Theta} + X^{(s),\rm opt}_{M,\rm exp})/2$, which is indeed our choice at LPA and NLO approximations. However, we apply further improvement to the NNLO result. Namely, we first apply the ansatz (22) on the NNLO dataset to extrapolate to the exponents corresponding to $M_{WHJ} \to \infty$, and after this step we compute the central value of the result from the regulators. We consider the values obtained this way to be our NNLO prediction, with the polynomial truncation improvement. Furthermore, we extrapolate our predictions at NNLO employing Wynn's epsilon algorithm whenever it is applicable, i.e., when the predictions at successive orders of the DE show an alternating behavior. We cited those extrapolated predictions in Table III.

(ii) One source of uncertainty originates from the choice of regulators, which we denote by $\Delta_{\rm reg}\overline{X}^{(s)}$ corresponding to the prediction $\overline{X}^{(s)}$. We define it to be half of the largest difference

$\Delta_{\rm reg}\overline{X}^{(s)}_M = |X^{(s),{\rm opt}}_{M,\Theta} - X^{(s),{\rm opt}}_{M,{\rm exp}}|/2$ between the two predictions obtained with different regulators. Considering empirical data, such as in Ref. [11], we see that the Θ_n-type regulator, with the smallest possible n at the given order in the DE yields predictions closest to the most precise ones, obtained from other methods. The exponential regulator (16), on the other hand, seems to produce predictions farthest from the most precise ones. This is true at least up to NNLO, which supports our choice for $\Delta_{\rm reg}\overline{X}^{(s)}$ at least up to NNLO of the DE.

(iii) Next, we compute the uncertainty of the DE according to Ref. [11], exploiting the hidden small parameter $1/4-1/9$ of the DE. Calling this source of error $\Delta_{\rm DE}\overline{X}^{(s)}$, we have $\Delta_{\rm DE}\overline{X}^{(s)} = |\overline{X}^{(s)} - \overline{X}^{(s-2)}|/4$, where $\overline{X}^{(s-2)}$ corresponds to the result from the previous order (∂^{s-2}) of the DE. Of course, this implies that we are unable to estimate the error from the DE at the LPA this way.

(iv) In addition to $\Delta_{\rm reg}\overline{X}^{(s)}$ and $\Delta_{\rm DE}\overline{X}^{(s)}$, the finite truncation M of the scale-dependent functions also introduces another source of systematic uncertainty $\Delta_{\rm poly}\overline{X}^{(s)}$. Every order of the DE introduces new scale-dependent functions F and thus additional sources of uncertainty if we truncate them. Thus we have $\Delta_{\rm poly}\overline{X}^{(s)} = \sum_{\{F\}}\Delta_F\overline{X}^{(s)}$ where we sum over all scale-dependent functions F available at the ∂^s order of the DE. We define these independent contributions as $\Delta_F\overline{X}^{(s)} = |\overline{X}^{(s)}_{M_F} - \overline{X}^{(s)}_{M_F-1}|$. We do this because we go so far in the polynomial expansion that $\Delta_F\overline{X}^{(s)}$ decreases monotonically for higher values of M_F. To estimate $\Delta_{\rm poly}\overline{X}^{(4)}$ at NNLO, we take the absolute difference between the data improved by (22). We have already elaborated in the main text that we apply the same degree of truncation to all scale-dependent functions corresponding to a given order of the DE. For instance, in the Z_2 symmetric models at NNLO, we have $\Delta_{\rm poly}\overline{X}^{(4)} = \Delta_U\overline{X}^{(4)} + \Delta_Z\overline{X}^{(4)} + \Delta_{WHJ}\overline{X}^{(4)}$. With the truncation used in this work, we have $\Delta_U\overline{X}^{(4)} < \Delta_Z\overline{X}^{(4)} \ll \Delta_{WHJ}\overline{X}^{(4)}$, so that $\Delta_{\rm poly}\overline{X}^{(4)} \approx \Delta_{WHJ}\overline{X}^{(4)}$.

(v) Finally, we have to combine the different sources of uncertainties in order to obtain the total uncertainties $\Delta\overline{X}^{(s)}$ quoted in the tables of the main text. There is no straightforward way to prove that the discussed sources are uncorrelated, so we decided to use a simple sum,

$$\Delta\overline{X}^{(s)} = \Delta_{\rm DE}\overline{X}^{(s)} + \Delta_{\rm reg}\overline{X}^{(s)} + \Delta_{\rm poly}\overline{X}^{(s)} \qquad \text{(B1)}$$

as a conservative estimate. As mentioned in point (ii) $\Delta_{\rm DE}\overline{X}^{(0)}$ is unavailable. Furthermore, $\Delta_{\rm reg}\overline{X}^{(0)} \gg \Delta_{\rm poly}\overline{X}^{(0)}$. Thus in practice we have $\Delta\overline{X}^{(0)} = \Delta_{\rm reg}\overline{X}^{(0)}$ at LPA. At the NLO $\Delta_{\rm DE}\overline{X}^{(2)}$ is the dominant source of uncertainty.

APPENDIX C: TECHNICAL DETAILS OF NUMERICAL COMPUTATIONS

We locate the Wilson-Fisher fixed point corresponding to the complete set of β functions ($\{\beta_{\tilde{g}_i} = 0\}$) for the dimensionless couplings $\tilde{g}_i$. In order to find the nontrivial root of this system of equations we have used the affine covariant Newton method with the iterative algorithm detailed in Secs. V and VI B. In the rare case it did not converge in 100 iterations we further applied the secant method. This requires two initial values; to obtain those we simply multiply the output from the affine covariant Newton method with 0.9 and 1.1.

The numerical integration of the threshold integrals L, M, and N (from Sec. III B) are computed with the optimized `NIntegrate` command of *Mathematica*, which selects the Gauss-Kronrod quadrature formula as the most efficient numerical integration method.

In every instance we have worked with 12 or more digits of precision in our numerical computations.

TABLE IV. The first two subleading scaling corrections ω_1 and ω_2 at the LPA, NLO, and NNLO of the DE for the O(N) symmetric models in $d = 3$ Euclidean dimensions. We have only kept the first few significant digits, which coincide for the predictions computed from the Θ regulator (13) and the exponential regulator (16).

N	Order of DE	ω_1	ω_2
0	LPA		3.3
	NLO	1.4	4.0
	NNLO	1.4	3.3
1	LPA		3.2
	NLO	1.7	3.9
	NNLO	1.7	3.2
2	LPA		3.1
	NLO	$1.9 \pm 0.1i$	3.6
	NNLO	1.8	3.3
3	LPA		3.0
	NLO	$2.0 \pm 0.5i$	3.5
	NNLO	1.9	3.4
4	LPA		2.94
	NLO	1.9	3.4
	NNLO	1.9	3.3
10	LPA		2.90
	NLO	1.96	2.8
	NNLO	1.96	2.9
100	LPA		2.99
	NLO	2.00	2.97
	NNLO	1.99	2.97

APPENDIX D: SUBLEADING SCALING CORRECTIONS

We also provide the scaling corrections $\omega < \omega_1 < \omega_2 < \ldots$ to the correlation length as discussed in Sec. III D. The smallest one ω is shown in Table II for the O(N) model at various N values. The larger scaling corrections ω_1, ω_2 are summarized in Table IV. Generally ω_n becomes more susceptible to the polynomial truncation with increasing n; ω_1, ω_2 are only stable in the first two or three significant digits with our employed truncation, detailed in Sec. VI B.

[1] C. Wetterich, Exact evolution equation for the effective potential, Phys. Lett. B **301**, 90 (1993).

[2] K. G. Wilson and J. Kogut, The renormalization group and the ϵ expansion, Phys. Rep. **12**, 75 (1974).

[3] M. Hasenbusch, Finite size scaling study of lattice models in the three-dimensional Ising universality class, Phys. Rev. B **82**, 174433 (2010).

[4] M. Hasenbusch, Monte Carlo study of an improved clock model in three dimensions, Phys. Rev. B **100**, 224517 (2019).

[5] R. Guida and J. Zinn-Justin, Critical exponents of the N-vector model, J. Phys. A: Math. Gen. **31**, 8103 (1998).

[6] O. Schnetz, Numbers and functions in quantum field theory, Phys. Rev. D **97**, 085018 (2018).

[7] M. V. Kompaniets and E. Panzer, Minimally subtracted six-loop renormalization of $O(n)$-symmetric ϕ^4 theory and critical exponents, Phys. Rev. D **96**, 036016 (2017).

[8] S. El-Showk, M. F. Paulos, D. Poland, S. Rychkov, D. Simmons-Duffin, and A. Vichi, Solving the 3D Ising model with the conformal bootstrap, Phys. Rev. D **86**, 025022 (2012).

[9] D. Simmons-Duffin, A semidefinite program solver for the conformal bootstrap, J. High Energy Phys. 06 (2015) 174.

[10] I. Balog, H. Chaté, B. Delamotte, M. Marohnić, and N. Wschebor, Convergence of Nonperturbative Approximations to the Renormalization Group, Phys. Rev. Lett. **123**, 240604 (2019).

[11] G. De Polsi, I. Balog, M. Tissier, and N. Wschebor, Precision calculation of critical exponents in the O(N) universality classes with the nonperturbative renormalization group, Phys. Rev. E **101**, 042113 (2020).

[12] D. F. Litim, Optimized renormalization group flows, Phys. Rev. D **64**, 105007 (2001).

[13] L. Canet, B. Delamotte, D. Mouhanna, and J. Vidal, Nonperturbative renormalization group approach to the Ising model: A derivative expansion at order ∂^4, Phys. Rev. B **68**, 064421 (2003).

[14] M. D'Attanasio and T. R. Morris, Large N and the renormalization group, Phys. Lett. B **409**, 363 (1997).

[15] See Supplemental Material at http://link.aps.org/supplemental/10.1103/PhysRevE.103.032135 for the code used in this work to derive the β functions and the explicit fixed point solutions at different polynomial truncations and regulators.

[16] P. M. Stevenson, Optimized perturbation theory, Phys. Rev. D **23**, 2916 (1981).

[17] L. Canet, B. Delamotte, D. Mouhanna, and J. Vidal, Optimization of the derivative expansion in the nonperturbative renormalization group, Phys. Rev. D **67**, 065004 (2003).

[18] K.-I. Aoki, K. Morikawa, W. Souma, J.-I. Sumi, and H. Terao, Rapidly converging truncation scheme of the exact renormalization group, Prog. Theor. Phys. **99**, 451 (1998).

[19] D. F. Litim, Critical exponents from optimised renormalisation group flows, Nucl. Phys. B **631**, 128 (2002).

[20] Z. Peli, S. Nagy, and K. Sailer, Effect of the quartic gradient terms on the critical exponents of the Wilson-Fisher fixed point in $O(N)$ models, Eur. Phys. J. A **54**, 20 (2018).

[21] P. Wynn, On a device for computing the $e_m(S_n)$ transformation, Math. Tables Aids Comput. **10**, 91 (1956).

[22] P. Graves-Morris, D. Roberts, and A. Salam, The epsilon algorithm and related topics, J. Comput. Appl. Math. **122**, 51 (2000); C. Brezinski, Numerical analysis in the 20th century Vol. II: Interpolation and extrapolation, *ibid.* **122**, ix (2000).

[23] N. Tetradis and C. Wetterich, Critical exponents from the effective average action, Nucl. Phys. B **422**, 541 (1994).

[24] G. v. Gersdorff and C. Wetterich, Nonperturbative renormalization flow and essential scaling for the Kosterlitz-Thouless transition, Phys. Rev. B **64**, 054513 (2001).

[25] N. Clisby and B. Dünweg, High-precision estimate of the hydrodynamic radius for self-avoiding walks, Phys. Rev. E **94**, 052102 (2016).

[26] N. Clisby, Scale-free Monte Carlo method for calculating the critical exponent γ of self-avoiding walks, J. Phys. A: Math. Theor. **50**, 264003 (2017).

[27] H. Shimada and S. Hikami, Fractal dimensions of self-avoiding walks and Ising high-temperature graphs in 3D conformal bootstrap, J. Stat. Phys. **165**, 1006 (2016).

[28] S. M. Chester, W. Landry, J. Liu, D. Poland, D. Simmons-Duffin, N. Su, and A. Vichi, Carving out OPEe space and precise O(2) model critical exponents, J. High Energy Phys. 06 (2020) 142.

[29] M. Hasenbusch and E. Vicari, Anisotropic perturbations in three-dimensional O(N)-symmetric vector models, Phys. Rev. B **84**, 125136 (2011).

[30] M. Hasenbusch, Eliminating leading corrections to scaling in the three-dimensional $O(N)$-symmetric ϕ^4 model: $N = 3$ and 4, J. Phys. A: Math. Gen. **34**, 8221 (2001).

[31] F. Kos, D. Poland, D. Simmons-Duffin, and A. Vichi, Precision islands in the Ising and $O(N)$ models, J. High Energy Phys. 11 (2016) 36.

[32] A. C. Echeverri, B. von Harling, and M. Serone, The effective bootstrap, J. High Energy Phys. 09 (2016) 097.

[33] Y. Deng, Bulk and surface phase transitions in the three-dimensional $O(4)$ spin model, Phys. Rev. E **73**, 056116 (2006).

[34] F. Kos, D. Poland, D. Simmons-Duffin, and A. Vichi, Bootstrapping the $O(N)$ archipelago, J. High Energy Phys. 11 (2015) 106.

[35] Y. Okabe and M. Oku, $1/n$ Expansion up to order $1/n^2$. III: Critical exponents γ and ν for $d = 3$, Prog. Theor. Phys. **60**, 1287 (1978).

[36] A. N. Vasil'ev, Y. M. Pis'mak, and Y. R. Khonkonen, 1/n Expansion: Calculation of the exponent ν in the order $1/n^3$ by the conformal bootstrap method, Theor. Math. Phys. **50**, 127 (1982).

[37] D. J. Broadhurst, J. A. Gracey, and D. Kreimer, Beyond the triangle and uniqueness relations: Non-zeta counterterms at large N from positive knots, Z. Phys. C **75**, 559 (1997).

[38] H. E. Stanley, Dependence of Critical Properties on Dimensionality of Spins, Phys. Rev. Lett. **20**, 589 (1968).

[39] P. de Gennes, Exponents for the excluded volume problem as derived by the Wilson method, Phys. Lett. A **38**, 339 (1972).

[40] G. Gaspari and J. Rudnick, n-vector model in the limit $n \to 0$ and the statistics of linear polymer systems: A Ginzburg-Landau theory, Phys. Rev. B **33**, 3295 (1986).

[41] This would be the case if we attempted to use (13) at N^{3}LO of the DE.